FOREX Publication
Open Access | Rapid and quality publishing

International Journal of
Electrical and Electronics Research (IJEER)
Research Article | Volume 13, Issue 3 | Pages 412-418 | e-ISSN: 2347-470X

Multirate Output Feedback Control for Enhanced Position Control of Rotary Servo Motion Plant (SRV02)

Hardik Kannad[1*], Hardik Patel[2], Rutvik Shukla[3], Ankur Gajjar[4], Manoj Khediya[5], Ankit Shah[6]

[1]*Assistant Professor, Instrumentation and Control Engineering Department, Government Engineering College, Rajkot, Gujarat, India; kannad.hardik@gmail.com*
[2]*Assistant Professor, Instrumentation and Control Engineering Department, Government Engineering College, Rajkot, Gujarat, India; er.hardik24@gmail.com*
[3]*Assistant Professor, Instrumentation and Control Engineering Department, Government Engineering College, Rajkot, Gujarat, India; rutvikshukla@gmail.com*
[4]*Assistant Professor, Instrumentation and Control Engineering Department, Shantilal Shah Engineering College, Bhavnagar, Gujarat, India; ankurgajjar.91@gmail.com*
[5]*Assistant Professor, Instrumentation and Control Engineering Department, Vishwakarma Government Engineering College, Ahmedabad, Gujarat, India; mdkhediya@vgecg.ac.in*
[6]*Assistant Professor, Instrumentation and Control Engineering Department, L. D. College of Engineering, Ahmedabad, Gujarat, India; ankitshah.ic@ldce.ac.in*

***Correspondence:** *Hardik Kannad; kannad.hardik@gmail.com*

ABSTRACT- This paper presents an experimental exploration of position control techniques applied to a Rotary Motion Servo Plant (SRV02), employing output feedback controllers. The transfer function model of the SRV02 is derived through first principles. Output feedback controllers, specifically Position Velocity (PV) and Multirate Output Feedback (MOF), are formulated and designed. The study evaluates the efficacy of these controllers in real-world scenarios for positioning control of the SRV02. A comparative analysis between PV and MOF controllers was conducted, assessing their static and dynamic characteristics. The results, obtained from both simulation and experimental setups, illustrate the superiority of MOF over PV controller in achieving precise position control of the SRV02. The findings of this study not only validate the effectiveness of MOF in position control applications but also provide insights into the practical implementation of output feedback controllers for enhancing the performance of rotary motion servo systems like SRV02.

Keywords: Servo plant, SRV02, Multirate output feedback, PV controller, Position control.

ARTICLE INFORMATION

Author(s): Hardik Kannad, Hardik Patel, Rutvik Shukla, Ankur Gajjar, Manoj Khediya, and Ankit Shah;
Received:05/02/25; **Accepted:** 15/07/25; **Published:** 25/08/25;
E- ISSN: 2347-470X;
Paper Id: IJEER 0502-11;
Citation: 10.37391/ijeer.130304
Webpage-link:
https://ijeer.forexjournal.co.in/archive/volume-13/ijeer-130304.html

Publisher's Note: FOREX Publication stays neutral with regard to jurisdictional claims in Published maps and institutional affiliations.

1. INTRODUCTION

The position control of a DC motor is crucial in various industrial applications such as robotics, manufacturing, and automation, where precise positioning of machinery or components is essential for maintaining quality, productivity, and safety standards [1-2]. In real-world scenarios, accurate position control ensures consistent product quality, reduces production time, minimizes waste, and enhances overall operational efficiency [3].

Position control of DC motors is commonly achieved through various techniques primarily based on single-rate output feedback. These methods entail utilizing feedback from sensors such as encoders or resolvers to continuously monitor the motor's position and adjust control signals accordingly. By employing a single feedback loop operating at a fixed sampling rate, these techniques effectively regulate the motor's position with respect to a desired reference point. Among these approaches, Proportional-Integral-Derivative (PID) control stands out as the most prevalent, offering a balance between simplicity and effectiveness in achieving stable and accurate position control [4-5]. Lead compensators anticipate the motor's response to control signals, enabling faster adjustments and improved transient response. Lag compensators, on the other hand, help reduce steady-state error by smoothing out the control signal [6]. State Feedback Control employs feedback from all or some of the system's state variables, such as position, velocity, and current, to determine the control signal [7-8]. By directly measuring these variables, it can achieve precise control and address nonlinearities in the system [9]. Model Predictive Control (MPC) utilizes a dynamic model of the motor to predict its future behavior and optimize the control signal over a finite time horizon. By considering future trajectories, MPC can effectively handle constraints and disturbances, leading to improved performance [10]. Sliding Mode Control (SMC) forces the system's state trajectory to converge to a predefined sliding surface, ensuring robustness against disturbances and uncertainties. Despite its effectiveness, it may lead to chattering in the control signal, which can affect system stability [11-12]. While single-rate output feedback techniques have proven successful in many applications, they may encounter challenges in addressing rapid changes in system dynamics or disturbances effectively [13].

As technology advances and demands for higher precision and responsiveness increase, there is growing interest in exploring alternative strategies such as multi-rate feedback control to further enhance the performance [14]. Multirate Output Feedback (MOF) introduces a novel approach by sampling the control input and sensor output of a system at different rates [15-16]. This method ensures closed-loop stability, a characteristic not guaranteed by static output feedback alone [17-18]. In MOF, either the control input or the sensor output is sampled at a faster rate than the other, allowing for dynamic adjustments [19]. This technique enables the realization of state feedback-based control laws of any structure by representing system states in terms of past control inputs and multi-rate sampled system output, offering a versatile and effective means of control.

The MOF technique leverages static output feedback to facilitate the simultaneous tuning of all control gains, addressing the limitations of traditional sequential tuning methods. This approach enables flexible pole placement while preserving a simple control structure, thereby streamlining the overall system design [20]. By integrating the simplicity of static output feedback with the versatility of pole assignment, the MOF framework offers a robust and adaptable solution for control design. Its effectiveness is further demonstrated through successful implementation in complex systems like magnetic levitation, even under mismatched uncertainties [21]. A novel approach for fast output sampling feedback control is presented, which leverages multirate sampling and static output feedback to achieve desired pole placement. This method enhances system performance and simplifies controller design by avoiding full state feedback requirements [22].

The present study investigates the Rotary Motion Servo Plant (SRV02) as the selected application. The Quanser SRV02 consists of a DC motor enclosed within a robust aluminum frame, coupled with a planetary gearbox. Additionally, it features sensors including potentiometers and encoders for position measurement, along with a tachometer for velocity measurement [23]. To enhance the position control of the SRV02, the MOF technique is introduced, with both simulation and experimental results presented. Furthermore, a comparative analysis is conducted to demonstrate the effectiveness of MOF in relation to Position Velocity (PV) control. In implementing MOF, the encoder output of the SRV02 undergoes sampling before generating the controller output. Specifically, for every four samples of encoder output, the controller output is generated. This setup ensures that the sensor's sampling rate is higher than that of the control action generated. Thus, MOF algorithms can significantly reduce the computational load compared to traditional single-rate control algorithms. By updating the controller at a lower rate than the plant, computational resources can be conserved without sacrificing control performance. This approach is not limited to the SRV02 system alone. Similar MOF strategies have been successfully applied to other systems such as magnetic levitation setups [21], unmanned ground vehicle (UGV) path tracking [24], active suspension systems [25], and networked multirate control applications [26]. These implementations validate the generalizability of the MOF technique to a wide range of industrial and networked control systems.

The paper is structured as follows: *Section 2* covers the methodology of MOF algorithm. In *section 3*, an in-depth exploration of the design of MOF controller is provided. *Section 4* presents the simulation and experimental findings related to the MOF controller, along with a comparative analysis between PV and MOF control approaches.

2. METHODOLOGY

Let's examine a dynamic system represented by,

$$\dot{x}(t) = Ax(t) + Bu(t)$$
$$y(t) = Cx(t) \qquad (1)$$

Where *A, B* and *C* represent the system matrix, input matrix and output matrix respectively. It is assumed that the *(A, B)* is controllable and the *(A, C)* is observable.

Fast Output Sampling (FOS), a subset MOF, is employed interchangeably throughout this paper. FOS entails sampling the system output at a frequency higher than that of the control input [21]. In this method, the control signal remains constant throughout each sampling interval τ, as illustrated in *figure 1*.

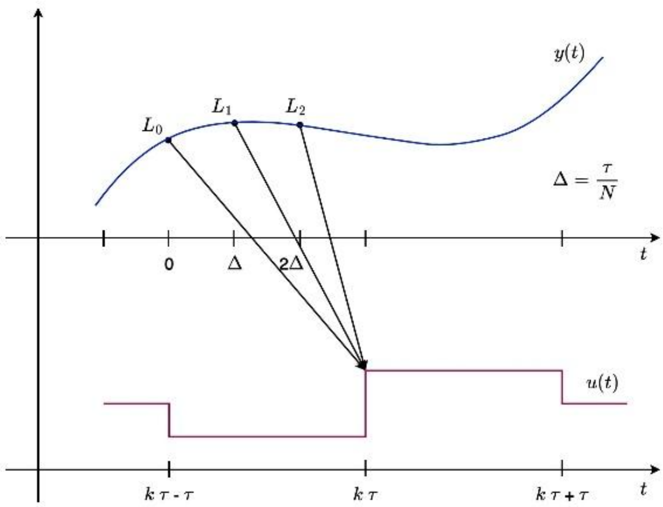

Figure 1. Visual representation showcasing the principle of fast output sampling

In *figure 1*, output measurements are obtained at intervals $t = l\Delta$, where $l = 0, 1, ..., N-1$, and the control signal is generated according to,

$$u(t) = Ly_k,\ k\tau < t \le (k+1)\tau \qquad (2)$$

Where gain matrix $L=(L_1 \quad L_2 \quad \cdots \quad L_N)$ and $y_k = (\,y(k\tau-\tau) \quad y(k\tau-\tau+\Delta) \quad \ldots \quad y(k\tau-\Delta))^T$. Here *1/ τ* is the rate at which the loop is closed, whereas output samples are taken at the *N*-times faster rate *1/Δ* [22].

Discretizing the system defined by *eq. (1)*, the sampled system is denoted by ($\emptyset_\tau$, Γ_τ, C) where *(A, B, C)* is sampled at a rate of *1/τ, i.e.*, $\emptyset_\tau = e^{A\tau}$, $\Gamma_\tau = \int_0^\tau e^{A\tau} ds\, B$. Considering the discrete-time system, at time *t=kτ*, the input is $u_k = u(k\tau)$, the state is $x_k = x(k\tau)$, and the output is y_k. Additionally, the system in *eq. (1)* is sampled with a sampling interval Δ=τ/N, where N is chosen to be an integer greater than the observability index of the system, and represented using the matrices Φ, Γ, and C. The discretized system is represented as follows:

$$x_{(k+1)} = \Phi_\tau x_k + \Gamma_\tau u_k$$

$$y_{(k+1)} = C_0 x_k + D_0 u_k \qquad (3)$$

Where $C_0 = (C \quad C\emptyset \quad \ldots \quad C\emptyset^{N-1})^T$ and

$$D_0 = \left(0 \quad C\Gamma \quad \ldots \quad C\sum_{j=0}^{N-2}\emptyset^j\Gamma\right)^T$$

Now, let's design the state feedback gain *F* to ensure that $(\emptyset_\tau + \Gamma_\tau F)$ has no eigenvalues at the origin, while achieving the desired closed-loop behavior.

$$u_k = F x_k \qquad (4)$$

$$x_k = (\Phi_\tau + \Gamma_\tau F)^{-1} x_{k+1} \qquad (5)$$

Utilizing *eq. (3)* and *eq. (5)*, we can express:

$$y_{k+1} = (C_0 + D_0 F)(\Phi_\tau + \Gamma_\tau F)^{-1} x_{k+1}$$

$$y_k = C(F,N) x_k \qquad (6)$$

Where $C(F,N) = (C_0 + D_0 F)(\emptyset_\tau + \Gamma_\tau F)^{-1}$ represents the fictitious measurement matrix.

The feedback control $u_k = L\, y_k$ can be viewed as static output feedback with a fictitious measurement matrix to incorporate the effect of F. Therefore, *L* must satisfy,

$$LC = F \qquad (7)$$

The *eq. (7)* allows for the realization of any state feedback gain using the FOS gain *L*. However, since *C(F, N)* may be a non-square matrix, the pseudo-inverse is employed to calculate its inverse. Nevertheless, this approach often results in a high output feedback gain *L*. To address this issue, the design of the output feedback gain *L* is accomplished using Linear Matrix Inequality (LMI) techniques. The following section outlines the controller design methodology discussed above, which is then implemented on the SRV02 plant.

3. CONTROLLER DESIGN

Given the plant's role in achieving control objectives, accurate modeling of the system becomes essential. Utilizing the SRV02 specifications and mathematical modeling provided in [23], the steady-state gain K = 1.53 (rad/sV) and time constant τ = 0.0254 (sec) are obtained. With these values, the transfer function of the SRV02 system can be derived as follows.

$$\frac{\Omega_l(s)}{V_m(s)} = \frac{1.53}{0.0254s+1} \qquad (8)$$

Here, $\Omega_l(s)$ represents the Laplace Transform of the SRV02 load shaft angular rate, and $V_m(s)$ denotes the laplace transform of the applied voltage to the SRV02 plant. Consequently, the laplace transform from the angular position of the load shaft $\theta_l(S)$ to the applied voltage to the SRV02 plant $V_m(S)$ can be expressed as:

$$\frac{\theta_l(s)}{V_m(s)} = \frac{1.53}{s(0.0254s+1)} \qquad (9)$$

The state-space representation of the above system is given by,

$$\dot{x}(t) = Ax(t) + Bu(t)$$

$$y(t) = Cx(t) \qquad (10)$$

Where, $A = \begin{pmatrix} -39.2927 & 1 \\ 0 & 0 \end{pmatrix}$, $B = \begin{pmatrix} 0 \\ 60.1280 \end{pmatrix}$ and $C = (1 \quad 0)$.

Following discretization, *eq. (10)* can be expressed as:

$$x_{k+1} = \emptyset x_k + \Gamma u_k$$

$$y_k = Cx_k \qquad (11)$$

Where ∅ and Γ represent the system matrix and input matrix respectively. The control signal is generated based on the following expression:

$$u_k = Le_k,\ k\tau < t \le (k+1)\tau \qquad (12)$$

Where *e* represents the error generated by algebraically subtracting the desired angular position y_d from the measured angular position y.

If the system output is sampled every Δ=0.0025 seconds and control signal input is applied every τ = 0.01 second, then the desired closed-loop poles at ±0.1414i can be achieved by calculating the state feedback gain *F* using the pole placement method.

$$F = (-115.7029 \quad -2.2762) \qquad (13)$$

Using the LMI approach, we obtained the FOS gain *L* from the *eq. (7)*, $LC = F$ as follows:

$$L = (4.7777 \quad 2.4581 \quad 0.8912 \quad 0.0066) \qquad (14)$$

Utilizing the aforementioned equations, the simulation is conducted, and the results are discussed in the subsequent section.

4. RESULTS AND DISCUSSION

In this section, the discussion revolves around both the simulation and experimental results. Furthermore, a comparison

International Journal of
Electrical and Electronics Research (IJEER)
Research Article | Volume 13, Issue 3 | Pages 412-418 | e-ISSN: 2347-470X

between the proposed MOF algorithm and traditional PV control is presented to establish the superiority of MOF over PV control.

4.1. Simulation Results

Within the Simulink environment, the architecture and functionality of the MOF controller are depicted in *figure 2*, illustrating its simulation diagram. In this control framework, the set-point is defined as ±30° away from the system's origin position. *Figure 3* showcases the real-time response of the SRV02 plant when subjected to control inputs from the MOF controller, visually representing both the angular position tracking and the control signal applied to achieve the set-point. It is noteworthy that throughout these operations, the voltage supplied to the motor remains consistently below ±10 V, demonstrating the motor remains within the operating limits. Performance evaluation of the system reveals key metrics: a peak time (Tp) of 0.23 seconds, indicating the time taken to reach the maximum deviation from the set-point; a peak overshoot (Mp) of 2.29%, reflecting the maximum deviation from the set-point during transient response; and a steady-state error (ess) of 0.00093 radians, signifying the deviation from the desired angular position once the system has stabilized.

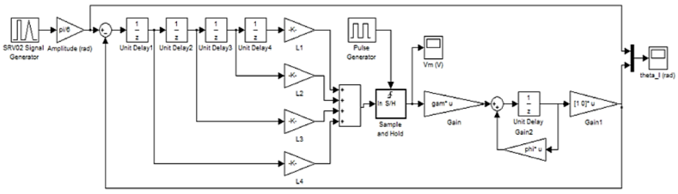

Figure 2. Simulink Diagram of MOF Controller

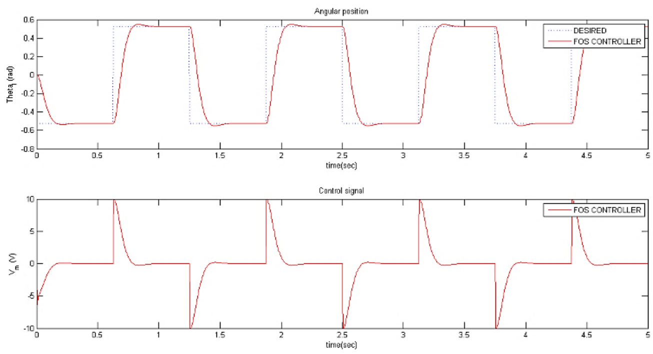

Figure 3. Simulation results: Performance of MOF controller for SRV02 plant

4.2. Experimental Results

Figure 4 illustrates a schematic diagram of the experiment conducted on the SRV02 system. In a typical feedback control system, essential components include the plant, sensors, actuators, and a controller. In digital real-time control applications, the analog controller is substituted by a digital computer (PC), providing the advantage of programmability to accommodate changes in design requirements or system dynamics.

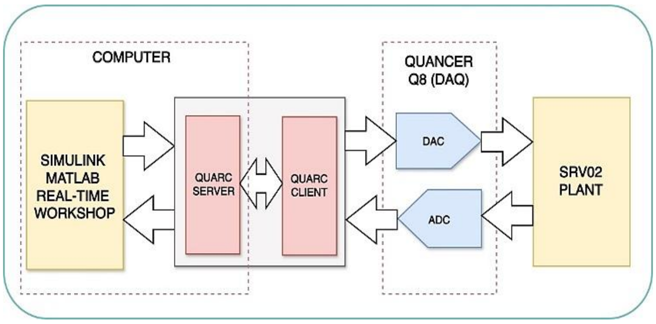

Figure 4. Schematic Diagram: Internal Configuration of SRV02 Plant

The application of the MOF controller for angular position control on the SRV02 plant necessitates the utilization of the experimental facility. This involves the intricate process of interfacing the hardware model with the Simulink diagram, a task efficiently accomplished through the QuaRC software. By leveraging QuaRC, the hardware and software components seamlessly integrate, enabling cohesive operation and real-time interaction. Furthermore, the development of the model is facilitated by the QuaRC library, complemented by the robust capabilities of the MATLAB/Simulink Real-Time Workshop. Together, these tools and frameworks empower researchers to bridge the gap between theoretical concepts and practical implementation, facilitating experimentation and validation in a controlled environment.

In this experimental setup, the continuous analog signal from the potentiometer undergoes conversion into discrete form through the DAQ and is subsequently measured by the HIL read. The control law is then computed within the Simulink environment and applied to the DC motor of the model using the HIL write. This conversion of the discrete form signal into a continuous form is facilitated by the DAC, as depicted in *figure 5*. Within this framework, the MOF controller aims to minimize the error signal between the measured angular position and the desired one. Notably, the control signal is updated at intervals of 0.0025 seconds (Δ) and applied to the control DC motor through the DAQ port of the Q8 terminal board at a slower rate of 0.01 seconds (τ).

The experimental study focuses on tracking the angular position of the load shaft of SRV02, with the results depicted in *figure 6*. Throughout the experiment, stringent measures are taken to ensure that the motor voltage remains below 10 V, guaranteeing optimal performance. The observed performance metrics include a *tp* of 0.172 seconds, indicating the duration taken to reach the maximum deviation from the desired set-point, and ess of 0.0134 radians. Remarkably, the *ess* is negligible, highlighting the accuracy of the control system. Moreover, the *Mp* is recorded at 5.21%, significantly lower than the desired *Mp* specification of 5%, affirming the effectiveness of the control strategy in achieving the desired control objectives.

FOREX Publication
Open Access | Rapid and quality publishing
International Journal of
Electrical and Electronics Research (IJEER)
Research Article | Volume 13, Issue 3 | Pages 412-418 | e-ISSN: 2347-470X

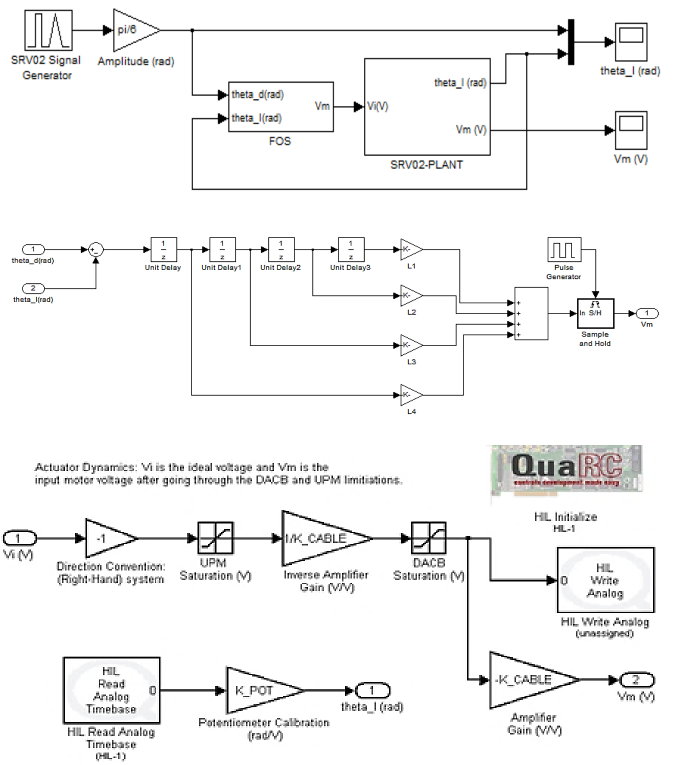

Figure 5. Simulink diagram illustrating MOF controller hardware interfacing

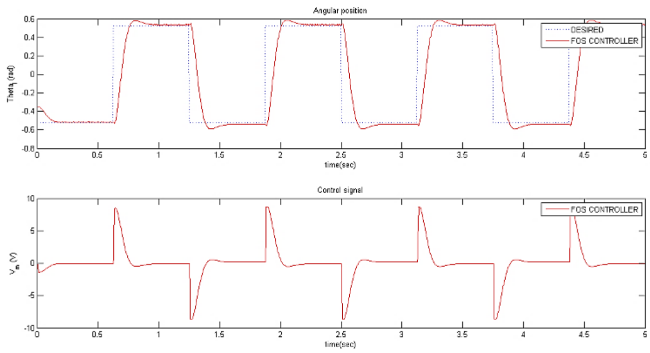

Figure 6. Experimental results: Performance of MOF controller for SRV02 plant

4.3. Comparative analysis

The proposed MOF controller is tested alongside a PV controller to assess its effectiveness. This comparative analysis entails examining both simulation and experimental outcomes derived from PV control and contrasting them with those of the MOF controller. Notably, the procedure for both simulating and experimenting with PV control mirrors that discussed for the MOF control scheme, ensuring a consistent evaluation framework. Leveraging the transfer function delineated in *eq. (9)*, the implementation of PV control is realized. To govern the angular position of the SRV02 load shaft, specific time-domain specifications are set, encompassing a target ess of 0, a desired *tp* of 0.20 seconds, and a maximum allowable *Mp* of 5.0%. For achieving this, the required proportional control gain and velocity gain are set as follows: *kp* = 7.82 (V/rad) and *kv* = -0.157 (Vs/rad).

Using the aforementioned gains, and with the set-point defined as ±30° from the system's origin position, simulations are conducted, and the results are illustrated in *figure 7*. The obtained results include a peak time of 0.2 seconds, a *Mp* of 5.99%, and ess of 0.00329 radians. However, the *Mp* exceeds the specified 5% *Mp* requirement, resulting in not all specifications being satisfied.

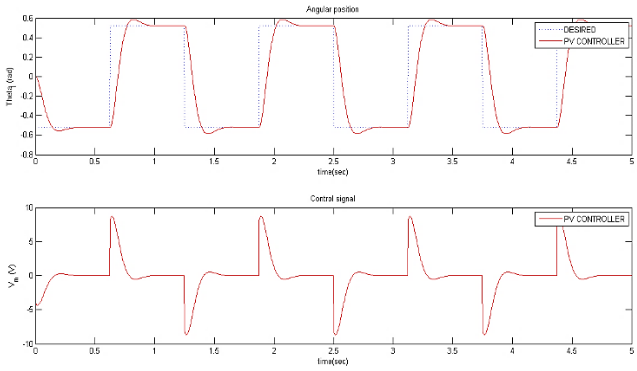

Figure 7. Simulation results: Performance of PV controller for SRV02 plant

The experiment aims to track the angular position of the SRV02 load shaft, with results depicted in *figure 8*, while ensuring the motor voltage remains below 10 V. The observed performance metrics include t_p of 0.152 seconds and e_{ss} of 0.00239 radians. However, the M_p is recorded at 14.20%, significantly exceeding the desired M_p specification of 5%. Despite the PV controller's fast response and negligible steady-state error, the high M_p deviates from the specified requirements.

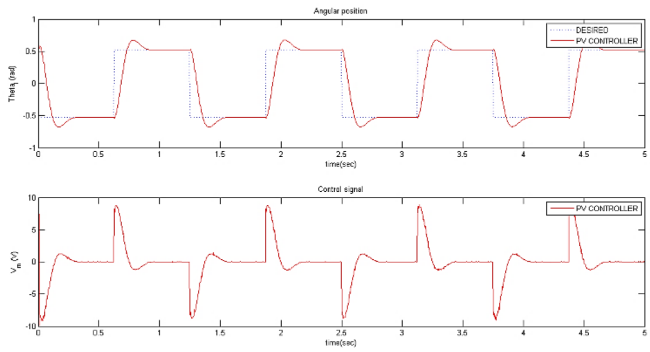

Figure 8. Experimental results: Performance of PV controller for SRV02 plant

The comparative analysis between the PV and MOF controllers is presented in *table 1*, encompassing evaluations based on both simulation and experimental results. This table provides a comprehensive overview of the performance of both controllers across various key metrics, allowing for a detailed examination of their effectiveness in controlling the system. Comparing the results from simulations and experiments helps understand how each controller works in different situations. This assists in selecting the most suitable control strategy for the given application.

Table 1. Comparison of PV and MOF controller performance: Simulation and experimental results

Performance parameter	PV Controller		MOF Controller	
	Simulation	Experimental	Simulation	Experimental
Peak time (t_p) (sec)	0.20	0.152	0.23	0.172
Peak overshoot (M_p) (%)	5.99	14.20	2.29	5.21
Steady-state error (e_{ss}) (rad)	0.00329	0.00239	0.00093	0.0134

Using the PV controller, overshoot is observed, with values of 5.99% in simulation and 14.20% in real-time experiments. To mitigate this overshoot, a MOF controller is designed and implemented. With the MOF controller, the overshoot is reduced to 2.29% in simulation and 5.21% in real-time experiments. However, it's important to note that the output feedback gain in the MOF controller is obtained from the state feedback, which relies on the system model. In real-time scenarios, obtaining a perfect model is challenging due to environmental factors and disturbances, leading to slight deviations in the performance of the MOF controller during real-time experiments.

5. CONCLUSION

This paper presents a detailed investigation into the MOF controller's efficacy in regulating the position of the SRV02 plant. By meticulously analyzing both simulated and experimental outcomes, the study demonstrates the MOF controller's superior performance compared to the conventional PV controller across various metrics. The comprehensive comparative analysis conducted on simulation and experimental data substantiates the MOF controller's enhanced capability in achieving desired control objectives. However, minor discrepancies observed between simulation and real-world experimental results underscore the influence of practical environmental factors. Despite these variations, the MOF controller consistently outperforms the PV controller in controlling the SRV02 plant's position. In future endeavors, researchers may consider exploring sliding mode control as a potential avenue for further refining control strategies, aiming to address challenges posed by real-world conditions and maximize control system performance in similar applications.

Conflicts of Interest: The authors declare no conflict of interest.

REFERENCES

[1] Arents, J.; Greitans, M. Smart Industrial Robot Control Trends, Challenges and Opportunities within Manufacturing. Applied Sciences 2022, 12 (2), 937. https://doi.org/10.3390/app12020937.

[2] Halwani, M.; Ayyad, A.; AbuAssi, L.; Abdulrahman, Y.; Almaskari, F.; Hassanin, H.; Abusafieh, A.; Zweiri, Y. A Novel Vision-Based Multi-Functional Sensor for Normality and Position Measurements in Precise Robotic Manufacturing. Precision Engineering 2024, 88, 367–381. https://doi.org/10.1016/j.precisioneng.2024.02.015.

[3] Zhu, D.; Feng, X.; Xu, X.; Yang, Z.; Li, W.; Yan, S.; Ding, H. Robotic Grinding of Complex Components: A Step towards Efficient and Intelligent Machining – Challenges, Solutions, and Applications. Robotics and Computer-Integrated Manufacturing 2020, 65, 101908. https://doi.org/10.1016/j.rcim.2019.101908.

[4] Kumar, R.; Sharma, V.; Kumar, V. Modelling and Comparative Analysis of Optimally Tuned PID Controllers in DC Motor Systems. 2024 Fourth International Conference on Advances in Electrical, Computing, Communication and Sustainable Technologies (ICAECT), Bhilai, India, January 11–12, 2024; IEEE, 2024. https://doi.org/10.1109/icaect60202.2024.10469200.

[5] RamaKrishnan, A.; Shunmugalatha, A.; Premkumar, K. An Improved Tuning of PID Controller for PV Battery-Powered Brushless DC Motor Speed Regulation Using Hybrid Horse Herd Particle Swarm Optimization. International Journal of Photoenergy 2023, 2023, 1–23. https://doi.org/10.1155/2023/2777505.

[6] Jalgham, F.; Zaggout, M.; Larbah, E. L. Design of Lead, Lag and Lead-Lag Compensators Based on Frequency Response Approach. The International Journal of Engineering & Information Technology (IJEIT) 2022, 8 (2), 56–61. https://doi.org/10.36602/ijeit.v8i2.150.

[7] Johan, K. Feedback Systems: An Introduction for Scientists and Engineers, Second Edition.; Princeton University Pres: S.L., 2021.

[8] Sanfelice, R. G. Hybrid Feedback Control; Princeton University Press, 2021.

[9] Ma'arif, A.; Setiawan, N. R. Control of DC Motor Using Integral State Feedback and Comparison with PID: Simulation and Arduino Implementation. Journal of Robotics and Control (JRC) 2021, 2 (5). https://doi.org/10.18196/jrc.25122.

[10] Elmorshedy, M. F.; Xu, W.; Fayez F. M. El-Sousy; Md. Rabiul Islam; Ahmed, A. A. Recent Achievements in Model Predictive Control Techniques for Industrial Motor: A Comprehensive State-of-The-Art. IEEE Access 2021, 9, 58170–58191. https://doi.org/10.1109/access.2021.3073020.

[11] Ma'arif, A.; Çakan, A. Simulation and Arduino Hardware Implementation of DC Motor Control Using Sliding Mode Controller. J Robot Control (JRC) 2021, 2, 582-587. https://doi.org/10.18196/jrc.26140.

[12] Hakan KIZMAZ. Comparative Analysis of Optimal Control Strategies: LQR, PID, and Sliding Mode Control for DC Motor Position Performance. Gazi university journal of science part a: engineering and innovation 2023, 10 (4), 571–592. https://doi.org/10.54287/gujsa.1393092.

[13] Shao, L.; Yang, J.; Li, S. Output Feedback Anti-Disturbance Control for Slow Sampled-Data Systems Combined with Model Predictive Control: An Alternating Predictive Observer Approach for Accelerating Sampling Rates. 2023 China Automation Congress (CAC), Chongqing, China, November 17–19, 2023; IEEE, 2023. https://doi.org/10.1109/cac59555.2023.10450784.

[14] Patel, A.; Purwar, S. Design of Event Trigger Based Multirate Sliding Mode Load Frequency Controller for Interconnected Power System. ISA Transactions 2022. https://doi.org/10.1016/j.isatra.2022.12.001.

[15] Shen, Y.; Wang, Z.; Dong, H.; Liu, H. Multi-sensor multi-rate fusion estimation for networked systems: Advances and perspectives. Information Fusion 2022, 82, 19–27. https://doi.org/10.1016/j.inffus.2021.12.005.

[16] Li, X.; Cheng, K.; Wang, Z.; Zhu, L.; Wei, G. Distributed interval observer-based robust control for multirate systems under the FlexRay protocol. Journal of the Franklin Institute 2024, 106708. https://doi.org/10.1016/j.jfranklin.2024.106708.

[17] Hadi, A. R. S.; Abaas, S.; Al-Modaffer, A. M.; Mawat, R. H. Enhancing Stability and Regulation of Output Voltage in Boost Converters with Learning Sliding Mode Control. Kufa Journal of Engineering 2024, 15 (3), 134–147. https://doi.org/10.30572/2018/kje/150308.

[18] Issa, A. H.; Baqir, H. F. Fault Detection and Isolation Based on Hybrid Sliding Mode Observer and Fuzzy Logic. Kufa Journal of Engineering 2021, 6 (1), 93–102. https://doi.org/10.30572/2018/kje/611316.

[19] Ahrens, J. H.; Xiaobo Tan; Khalil, H. K. Multirate Sampled-Data Output Feedback Control with Application to Smart Material Actuated Systems. IEEE Transactions on Automatic Control 2009, 54 (11), 2518–2529. https://doi.org/10.1109/tac.2009.2031204.

[20] Rehimi, S.; Bevrani, H.; Urabe, C. T.; Kato, T. Grid Forming Converter Control System Synthesis: A Static Output Feedback Approach. IEEJ Transactions on Electrical and Electronic Engineering 2024. https://doi.org/10.1002/tee.24063.

[21] Vernekar, P.; Bandal, V. Sliding mode control for magnetic levitation systems with mismatched uncertainties using multirate output feedback. International Journal of Dynamics and Control 2023. https://doi.org/10.1007/s40435-023-01151-3.

[22] Janardhanan, S.; Bandyopadhyay, B. A new approach for the design of fast output sampling feedback controller. 1st National Conference on Instrumentation & Control (ICECON'03), 2003.

[23] Apkarian, J.; Lévis, M.; Gurocak, H. USER MANUAL SRV02 Rotary Servo Base Unit Set up and Configuration Developed By. https://nps.edu/documents/105873337/0/SRV02+Base+Unit+User+Manual.pdf/ce50a48e-d169-4652-a9df-ae979af10094?t=1441916178000 (accessed 2024-05-18).

[24] Salt, J.; Alcaina, J.; Cuenca, Á.; Baños, A. Multirate control strategies for avoiding sample losses. Application to UGV path tracking. ISA Transactions 2020, 101, 130–146. https://doi.org/10.1016/j.isatra.2020.01.025.

[25] Chen, G.; Zhu, M.; Xia, J.; Park, J. H. Fuzzy Dynamic Output Feedback for Networked Control Active Suspension Systems: An IQC-Based Heuristic Multirate Sampling Iterative Controller Algorithm. IEEE Transactions on Industrial Electronics 2024, 1–11. https://doi.org/10.1109/tie.2024.3493207.

[26] Zhang, Y.; Zou, L.; Song, B.; Zhao, Z.; Wang, Y. Neural-network-based output feedback control for networked multirate systems: A bit rate allocation scheme. Information Sciences 2023, 637, 118952. https://doi.org/10.1016/j.ins.2023.118952.